

International Journal of
**Applied
Ceramic
TECHNOLOGY**

Ceramic Product Development and Commercialization

The Use of Sphere Indentation Experiments to Characterize Ceramic Damage Models

R. Brian Leavy*

U.S. Army Research Laboratory, Aberdeen, Maryland 21005

Rebecca M. Brannon

Mechanical Engineering, University of Utah, Salt Lake City, Utah 84112

O. Erik Strack

Sandia National Labs, Albuquerque, New Mexico 87185

Sphere impact experiments are used to calibrate and validate ceramic models that include statistical variability and/or scale effects in strength and toughness parameters. These dynamic experiments supplement traditional characterization experiments such as tension, triaxial compression, Brazilian, and plate impact, which are commonly used for ceramic model calibration. The fractured ceramic specimens are analyzed using sectioning, X-ray computed tomography, microscopy, and other techniques. These experimental observations indicate that a predictive material model must incorporate a standard deviation in strength that varies with the nature of the loading. Methods of using the spherical indentation data to calibrate a statistical damage model are presented in which it is assumed that variability in strength is tied to microscale stress concentrations associated with microscale heterogeneity.

Introduction

Numerical modeling tools have long been used to capture the behavior of ceramics in armor systems. For example, seminal constitutive modeling work of

*Brian.Leavy@utah.edu

Johnson and Holmquist¹ has established an essential foundation for describing ballistic failure of ceramics. The present work aims to extend this class of model by incorporating the effect of microscale heterogeneity that leads to pressure dependence of failure mechanisms. Without such enhancements, a ceramic model that is tuned to match one experiment often fails to predict the results in a different application.²

The ceramic experiments of Hauver *et al.*,³ Lundberg and Lundberg,⁴ Orphal and Franzen,⁵ and Anderson *et al.*⁶ provide penetration rates and other time-varying target failure information. These time-resolved experiments are used to calibrate the damage model parameters (such as strain-to-failure or failure energy) that are associated with the progression of failure from its initiation to complete loss in strength.⁷ Failure initiation itself begins at statistically distributed weak points in the material, thus requiring statistical spatial variability in strength that is proposed here to be parameterized via spherical indentation experiments. Specifically, the cracking patterns observed in spherical indentation data indirectly quantify microheterogeneity.

The evolution of damage in ceramics due to projectile impact has been studied extensively in the past. Excerpts from ceramic society proceedings such as Sagamore⁸ and PacRim,⁹ contain extensive references. Normandia and Gooch¹⁰ reviewed earlier attempts to screen ceramics using sphere impact tests by Donaldson *et al.*¹¹ and Donaldson and McDonough¹² and critiqued by Sternberg.¹³ Low-velocity impacts using tungsten carbide (WC) spheres to generate damage were presented by Shockey *et al.*¹⁴ and Kim *et al.*¹⁵ for ceramic targets. Historical references of high-velocity penetration using WC data appear in Herrmann and Jones,¹⁶ Goldsmith,¹⁷ and Martineau *et al.*¹⁸ There are a number of helpful reviews by Lawn,¹⁹ Stronge,²⁰ and Fischer-Cripps *et al.*²¹ For damage analyses, there is a useful overview of ceramic impacts by Tanabe *et al.*²² The current paper extends the previous ceramic failure analysis with modeling techniques that incorporate experimentally observed variability and size effects.²³

The indentation experiments presented in this paper examine the ceramic damage morphology of simplified low-velocity projectile impacts. WC spheres with velocities between 50 and 500 m/s impact ceramic targets in metal cups. Ceramic targets consist of silicon carbide (SiC) and boron carbide (B₄C). These generic screening experiments allow for a detailed analysis of specific materials of interest, with the overall goal being

a connection of the ballistic performance to statistically varying material properties.

The sphere impact tests are used to calibrate a new ceramic model, called Kayenta, currently implemented in the shock-physics finite-element code ALEGRA.²⁴ This model is an extension of the Sandia GeoModel²⁵ that was originally developed for geological materials, but has been enhanced to include scale-dependent statistical damage for ceramics and metals.²⁶ Scale dependence and statistical variability are included not only to reduce mesh sensitivity but also to improve predictive capability by providing a distribution of weak points that give rise to localized cracking.²⁷

The Kayenta model in ALEGRA uses a new failure distribution methodology that shares similarities to classical Weibull²⁸ theory in hydrostatic tension but which smoothly deviates from Weibull theory for other loading paths that involve shear. A Weibull distribution is used merely as an option that can be replaced with other distributions if necessary. This approach uses not only the material properties measured from laboratory experiments but also the length scales associated with the particular experiments. Volume scaling concepts similar to the work of Bažant and Planas²⁹ Bažant³⁰ and Trustrum and Jayatilaka³¹ are implemented at the finite element level.

Accounting for the size effects of strength helps mitigate mesh dependency problems. Moreover, incorporating spatially variable strengths automatically results in an “event horizon” effect in which increasing the strain rate causes an increase in the number of fractures because of the finite time required for release waves to propagate through the material.³²

To parameterize the new material model, the dynamic characterization work of Grady,³³ Vogler *et al.*,³⁴ and Dandekar³⁵ is used. Additionally, the compilations of Holmquist *et al.*³⁶ are an essential starting point. The original high pressure yield surface calibration is based on the Johnson–Holmquist (JH) ceramic models.³⁷ The Kayenta model’s completely failed material behavior involves concepts similar to the work of Duncan³⁸ and Anderson and Chocron.³⁹ Traditional quasi-static tests conducted by A. A. Wereszczak (personal communication) and others provide additional invaluable information. The failure distributions used in the Kayenta model stem from the actual measured uncertainty in the characterization experiments. New experiments were completed at the Sandia National Labs⁴⁰ to obtain measurements of the failure surface under triaxial loading

conditions, an area of the failure surface where no data were available.

Methods

The Kayenta Model

Kayenta strikes a balance between first-principals micromechanics and phenomenological, homogenized, and semiempirical modeling strategies.⁴¹ A set of standard strength experiments (e.g., plate impact, triaxial compression [TXC], diametral compression) is used to set model parameters. Uncertainty observed in these experiments, as well as variability in crack patterns for spherical indentation, are used to set values for the scale effects and statistical parameters (a complete derivation and analysis of this new method is presented in Brannon and Strack⁴²). Once these parameters have been determined, ballistic experiments are used to calibrate additional parameters in the model.

Like the JH ceramic model, as well as other classical damage models,⁴³ Kayenta allows the stress to reach a pressure-dependent limit threshold surface that then collapses with damage down to a completely failed strength surface that is similar to that of sand or gravel. Unlike the JH model, which imposes a fixed strain-to-failure, Kayenta imposes a scale-dependent time to failure that indirectly regulates the energy of failure. Kayenta also includes the third-invariant dependence as well as porosity effects in its yield surface; see Fig. 1. The Kayenta limit surface in TXC specifies shear strength τ dependence on pressure p according to

$$\tau = Y[1 - e^{-s(p+h)/Y}] \tag{1}$$

where the material parameters are the high-pressure limit strength Y , the hydrostatic tensile strength h , and the initial slope s at the hydrostatic tensile limit. Any of these parameters can be varied statistically and still generate a convex surface. The addition of uncertainty to the yield function is another distinguishing feature of the Kayenta model. Kayenta’s spatially variable probability functions incorporate uncertainty in flaw size and orientation of the macroscopically homogeneous material. Through proper scaling, the behavior is captured in the fuzzy failure boundary theory that incorporates length scales to mitigate mesh dependence.⁴⁴ The failure distributions predict that larger volumes are inherently weaker and fail earlier than smaller ones due to the probability of critical flaws (Fig. 2).

The Weibull distribution is applied to the horizontal pressure axis of Fig. 2 with \bar{h} , which is the peak strength in hydrostatic tension. The parameter to be perturbed, in this case the initial peak h value, is implemented at the finite element level by the following equation:

$$h = \bar{h} \left[\frac{\bar{V} \ln R}{V \ln(1/2)} \right]^{1/m} \tag{2}$$

where \bar{h} is the median value of the property h as measured using a sample volume \bar{V} , R is a random number, and m is the Weibull modulus quantifying the observed variability in the material property. The Weibull distribution is seeded about the median value for the material, with the value adjusted for the finite element volume V . A random distribution of R values is used for the elements, with the overall average being a factor

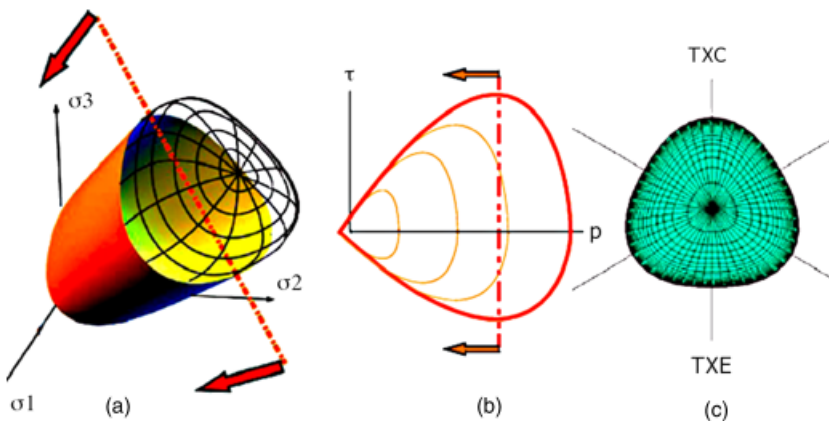


Fig. 1. (a) Yield surface with a high-pressure cap shown as a wireframe. (b) Meridional side view, with the hydrostat as abscissa. (c) Noncircular octahedral profile allowing for well-known extension-compression differences in brittle strength.

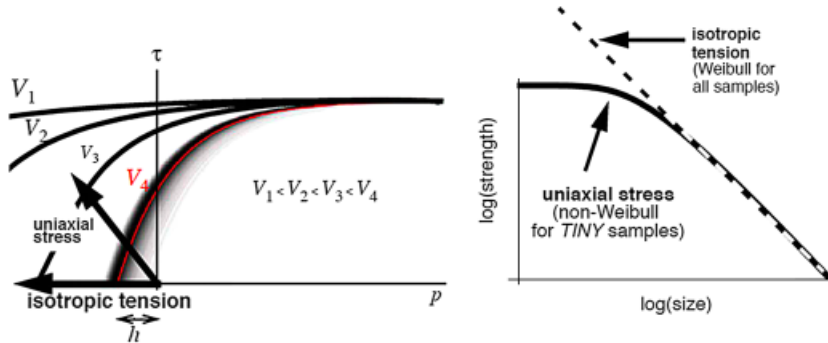


Fig. 2. The Weibull scale effect is applied only on the pressure intercept. The curved lines on the left plot are median limit surfaces for different specimen volumes showing that, as shown in the plot on the right, strength remains bounded for any stress path, such as uniaxial stress, having a deviatoric component.

of the median, the finite element volumes, and the Weibull modulus. As seen in Fig. 2, while the hydrostatic tension h can increase without bounds, the values of τ approaches the limit value of Y . In this way, the model implementation incorporates observed behavior seen in the characterization experiments.

Experimental Parameterization

A traditional yield model presumes that shear strength is a deterministic scale-insensitive function of pressure. The Kayenta model incorporates observed variability in strength so that the failure threshold is replaced by an uncertainty band centered about a scale-sensitive median curve.

As illustrated in Fig. 3, the observed degree of variability decreases with increasing pressure, thus giving a

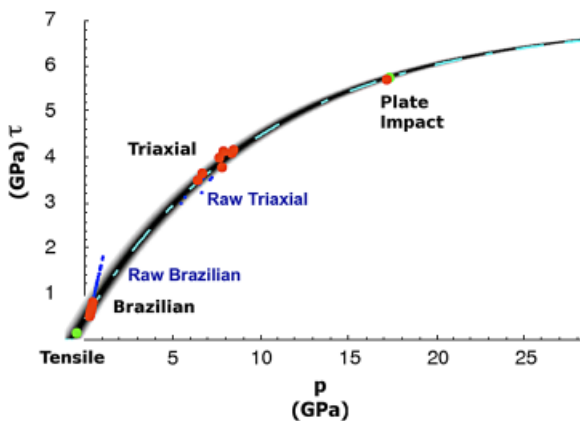


Fig. 3. Meridional view of the Kayenta material model and experiments for silicon carbide.

thick uncertainty band at low pressure that becomes increasingly thin with increased confinement. For example, in the high-pressure plate impact experiments, there is very little variability, corresponding to a large Weibull modulus.³⁴ In low-pressure Brazilian tests performed at Sandia (see Fig. 4), the Weibull modulus is 8.3. Figure 3 also incorporates normalization of the data to a common reference scale. Namely, if strength measurements are performed using a specimen volume V , then referring to Eq. (2), Weibull theory predicts that strength measured using a reference sample volume \bar{V} is different by a factor of $(\bar{V}/V)^{1/m}$. Raw experimental values for a variety of specimen sizes are displayed as small blue dots in Fig. 3, and larger red dots show the same data scaled to a common reference.

To date, the primary experiments validating a scale effect in SiC have been diametral compression, or Brazilian experiments. Cylinders ranging between 3.175

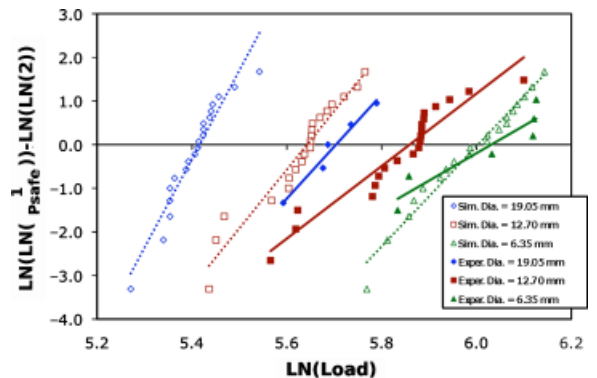


Fig. 4. Brazilian Weibull distribution and volume scaling of silicon carbide.

and 25.4 mm in diameter are quasi-statically compressed between two platens until failure.

Figure 4 illustrates the importance of uncertainty and scale effects. The abscissa is Brazilian failure strength on a logarithmic scale. The ordinate is a double-logarithmic transformation of the probability that the sample is safe from failure (P^{safe}). The solid filled measured data points are fitted to solid straight lines in which the slope equals the Weibull modulus. One colored line and symbol set was drawn for each of the three different sample diameters tested. The corresponding hollow data points and dashed lines are simulations using the Kayenta damage model with statistics and scale effects. The simulations predict the right trend of an increase in strength and a decrease in slope as the specimen size decreases. Upon inspection of the simulation results, it is clear that they are highly mesh sensitive. Efforts to resolve this numerical verification issue have included alternative volume scaling formulations, and work is underway to investigate its ties to energy release rates as well as under-resolution of stress associated with low order shape functions in the finite element model.

Triaxial compression and extension tests provide additional information about the yield surface and variability of brittle materials. Somewhat a misnomer, “triaxial” refers to an axisymmetric stress state having two equal eigenvalues. For TXC, the axial stress (single eigenvalue) is more compressive than the lateral stresses (dual eigenvalues). For triaxial extension (TXE), the axial stress is less compressive than the lateral stresses. In most cases, all the stresses in TXE are compressive, despite the use of the term “extension” in the name of the test. Strength in unconfined uniaxial tension is orders of magnitude smaller than in TXC. This effect can be modeled purely through the pressure dependence of strength. However, at low pressures, the strength of rock is strongly dependent on the third stress invariant. Specifically, when comparing TXE and TXC *at the same pressure*, data show that the equivalent shear stress at failure in TXC can be as much as twice as large as that in

TXE. This observation requires limit surface shapes that have strong triangular octahedral profiles at low pressure as illustrated in Fig. 1. Consistent with observations for quasi-brittle materials, the Kayenta model allows the octahedral profile to smoothly transition from a triangle (corresponding to a maximum principal stress or strain criterion) at low pressure to a circle (corresponding to a von Mises or Drucker–Prager yield model) at high pressure.

Plate impact experiments probe the high-pressure regime of the model. As line Visar experiments, in which multiple points of data are recorded, become more prevalent,⁴⁵ more statistical information can be discerned from a single test. The current series of experiments by Vogler *et al.*³⁴ supplement strength and pressure data consistent with previous work. These experiments provide controlled model parameterization data in a regime that exists in many dynamic ballistic experiments.

Ballistic Experiments

In this study, ballistic impact experiments up to 500 m/s are conducted on SiC and B₄C ceramics using WC spheres. The test procedure consists of firing 6.35-mm diameter spheres launched in a sabot from a gas gun. The WC spheres contain 6% cobalt by volume, with a nominal density of 14.90 g/cm³. Time is measured between two lasers at the end of the barrel to determine velocity, or with two orthogonal pairs of 150 keV X-ray radiograph systems. The target consists of a 25.4-mm diameter and length ceramic cylinder, manufactured by BAE Systems (Vista, CA). The two materials tested are SiC (SiC-N) and B₄C. Table I has a summary of the material properties for the target materials.

The ceramic is slip-fit inside a 6.35-mm walled titanium alloy cup, which is held in place by a rigid structure. The opening of the cup allows the sphere impactor to strike the ceramic face directly. The cup keeps the damaged ceramic in place for posttest examination.

Table I. Ceramic Target Properties

Material	Density (g/cm ³)	Grain Size (μm)	Young's Modulus (GPa)	Poisson's Ratio	Knoop Hardness (GPa)	Fracture Toughness (MPa m ^{1/2})	Flexure Strength (MPa)	Polytype
SiC-N	3.22	3.3	452	0.165	18.6	5.1	620	6H, 15R
B ₄ C	2.52	15.0	465	0.170	18.9	2.9	450	B ₄ C, C

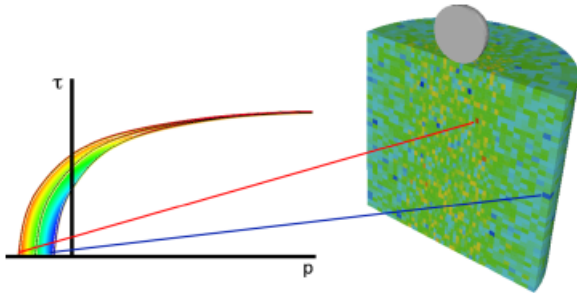


Fig. 5. Relation of model variability and element seeding in dynamic indentation simulations.

A significant benefit of this technique is material recovery for microscopic, X-ray computed tomography, and cross section analyses. These experiments can be used to calibrate the Kayenta model's damage evolution and variability parameters.

Figure 5 illustrates the relationship between the model implementation of variability, and an actual simulation of the ballistic impact experiments. Lagrangian finite elements in the ceramic target on the right are colored by the seeded tensile strength h . The red color corresponds to Weibull seeded elements with the highest tensile strength (the largest negative values on the pressure axis in Fig. 5). These elements have the greatest strength based on the Weibull deviation from the median (green) values. As can be seen in the figure, the target appears to be mostly green, corresponding to the median strength of the material. Blue elements in the target correspond to weaker elements, which used the lower blue curve of the model.

In addition, the radial mesh used in this example has slightly smaller elements in the center of the simulation, with larger elements near the outer edge of the target. The volume scaling of the material strength in these elements is witnessed by the greater accumulation of higher strength (yellow and red) in the middle of the simulation. By relating the element size and all model calibration to a common reference volume, the simulation will accurately predict the material performance differences in a simulation that models a sample with 1 mm^3 elements versus one with cubic meter wide elements.

Incorporation of statistics and scale effects significantly mitigates mesh size sensitivity in dynamic indentation problems, which have been reported to have severe mesh texture bias in glass indentation simulations.⁴⁶

Figure 6 shows the same 500 m/s impact simulation of SiC run with three different mesh sizes. Damage



Fig. 6. Mitigating mesh dependency in three different resolution silicon carbide indentation simulations. Larger to smaller mesh sizes shown from left to right.

(light colored elements) occurs in roughly the same locations and at the same time in all three mesh resolutions. However, a similar reduction in mesh sensitivity was not observed in Brazilian testing, even at high rates. The contrast between this mixture of positive and negative results indicates that proposed methods for limiting mesh sensitivity should be demonstrated to be effective under a variety of loading scenarios using a single material parameter set.

Results and Discussion

The ballistic impact experimental calibration and validation involves recording the failure morphology of a variety of simplified ballistic impact events. Figure 7 is a labeled overlay of the experimental results from a cross sectioned SiC target impacted at 375 m/s.

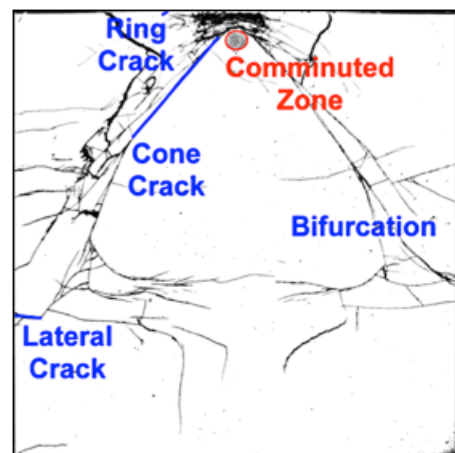


Fig. 7. Crosssectioned silicon carbide specimen with highlighted features.

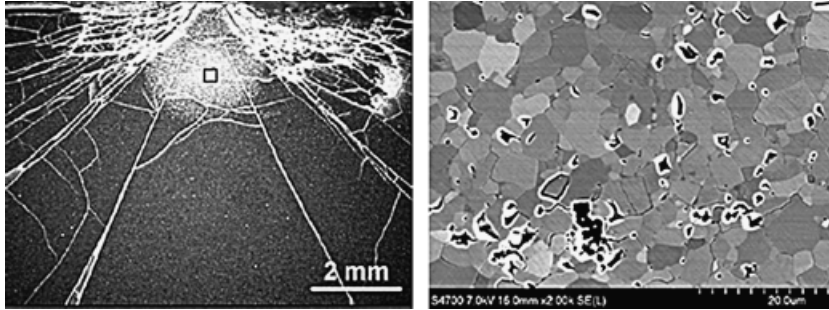


Fig. 8. Silicon carbide cross section of 500 m/s impact (left) and zoom in of comminuted zone (right).

Lateral cracks in Fig. 7 branch out horizontally from the cone cracks that originate at the impact point. A ring crack is essentially a circular crack that, along with radial cracks, is visible from the top surface. In addition, for SiC, a visual damage region forms between the major cone cracks directly under the impact point. This comminuted region consists of a dense population of microcracking between the grain boundaries, as well as grain pullout as seen in Fig. 8.

As observed in the experiments, the comminuted region is less noticeable in the extremely low velocity impacts. Moreover, the existence of a comminuted region appears to be material dependent.^{47,48}

The cone cracking distributions and angles are also of interest in determining how the material will fail dynamically. As the impact velocity increases, the angle (measured from the horizontal) and number of cone cracks increases substantially. If the thickness of the ceramic is decreased or if the projectile impulse is increased, the cone cracks eventually become vertical.

Several samples have also been analyzed using X-ray computed tomography.⁴⁹ The potential to analyze the results in a nondestructive manner and to generate 3D image maps of experiments makes this method very attractive. It is possible, for example, to measure the angle of the major cone crack in one 385 m/s impact for all 360°, which is approximately 66° from vertical.

Macroscopically, the radial cracking of specimens is another failure mode of interest in determining how a ceramic will perform in a ballistic event. Radial cracks serve as symmetry breakers, which can be realistically modeled by the introduction of variability, volume scaling, and by including the low-pressure strength differences discussed earlier. Figure 9 is an example of the radial cracking seen in experiments and simulations with SiC. Without the incorporation of variability in the simulations, the ceramic material model would behave the same. As such, when failure occurs, it catastrophically fails everywhere at once, effectively removing the brittle failure capabilities that may be incorporated in a

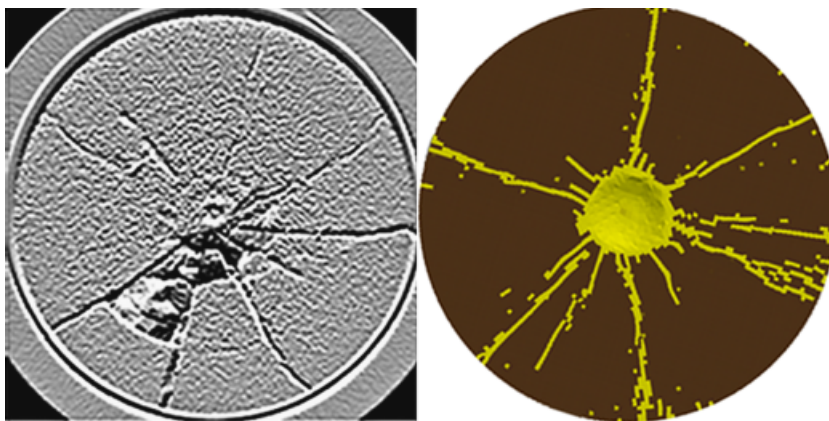


Fig. 9. X-ray computed tomography image of top surface cracking (left) and corresponding simulation (right) from a 385 m/s impact of silicon carbide.

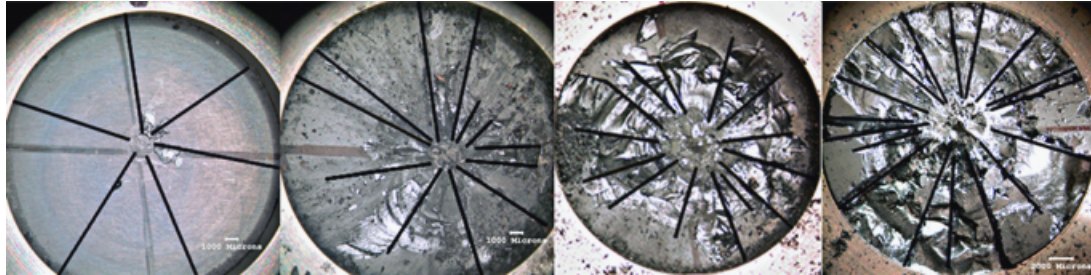


Fig. 10. Increase in radial cracking in boron carbide experiments due to an increase in impact velocity from 100 m/s (left) to 400 m/s (right).

material model. By including variability, the numerical issues that hinder most simulations are mitigated and the model can react as designed.

As seen in the experiments in Fig. 10, the number of radial cracks increases with an increase in impact velocity. The Kayenta model accurately predicts an increased frequency of cracks as impact velocity increases because the release waves initiated by failing elements are captured by the underlying finite element method. As the impact velocity is increased, the release waves, which have a constant velocity, are increasingly incapable of shielding the material from the growth of additional cracks.

The Kayenta model in ALEGRA preserves the completely failed material in the mesh, which still has strength, and can be recompressed. Currently, the material model yield surface for SiC and B₄C softens down to a material with a slope similar to that of gravel or sand.⁵⁰ The rate of the limit surface collapse is based on crack speeds and the corresponding element volumes such that the energy release rate is relatively mesh insensitive.

The simulations in Fig. 11 represent preliminary results of a Kayenta material model for B₄C. The JH

model for B₄C⁵¹ is used as a starting point for defining the median limit surface to be used in the Kayenta model. The Kayenta model requires an input of the time it takes for a sample of the reference volume to soften completely. It is assumed that these times are proportional to the crack growth speed. Approximate crack speeds determined by Ramesh and colleagues^{52,53} are used for both SiC and B₄C. A value of 10% of the longitudinal wave speed is used for SiC, and 3.5% for B₄C. The relationship between these values and the actual speeds generated by the model is yet to be determined, and future revisions of the model may allow direct specification of the crack-growth speed.

Sphere indentation experiments with B₄C exhibit a greater frequency of both radial cracking, as well as lateral and cone cracking, when compared with SiC. Using a higher Weibull modulus of 10, along with the lower crack speed mentioned above in the B₄C model results in a good match to the experimental results. The effect of changing the Weibull modulus is shown in Fig. 11. As the Weibull modulus increases, the variability is reduced, and the material is more likely to fail at multiple locations at once when the material is quickly loaded in the impact event.

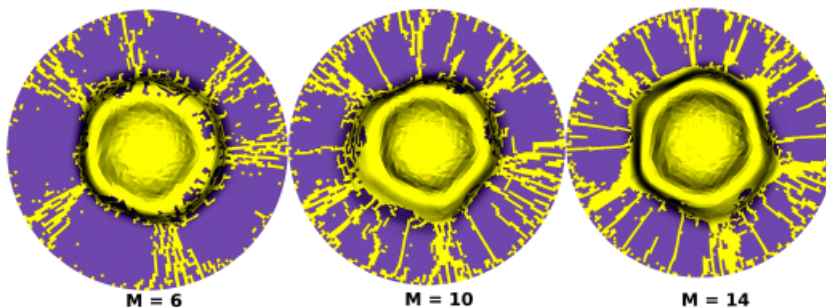


Fig. 11. Weibull modulus effect on radial cracking in boron carbide simulations impacted at 400 m/s.

This indicates that it may be possible to use these types of experiments to calibrate both the rate parameters and the variability parameters. The authors hope to obtain characterization experiments of B_4C similar to those completed for SiC to confirm this result.

Conclusions

In this paper, dynamic indentation experiments have been assessed for their usefulness in calibration and validation of ceramic material models that account for uncertainty and scale effects in material strength. Sphere impact experiments between 50 and 500 m/s are conducted, which promote damage and failure initiation, without substantial penetration or complete target failure. Silicon carbide and B_4C ceramic targets are analyzed through cross sections and X-ray computed tomography.

The number of radial cracks observed in the dynamic indentation offers a means of calibrating variability in strength and the rate of the progression of damage. Changes in the character of cone and lateral cracking that occur as impact velocity increases may serve as validation for damage models, provided the experiments are not used for the initial calibration.

The Kayenta model has been used as a means of exploring nontraditional features in modeling dynamic failure of ceramics. For example, third invariant dependence allows the failure criterion to transition smoothly from a principal stress criterion at low pressures to capture brittle failure behavior, to a more traditional von Mises plasticity profile at high pressures. This limit surface profile is statistically perturbed to reproduce observed experimental variability in strength that is pronounced at low pressure and is strongly scale dependent. Softening and damage is modeled by allowing the Kayenta limit surface to collapse to a failed surface that is representative of sand or gravel. Calibrating Kayenta's scale-sensitive time-to-failure criterion requires time-resolved failure data to supplement the dynamic indentation data.

Mesh sensitivity continues to undermine the predictive capability of damage models. Incorporation of scale effects and uncertainty dramatically reduces mesh sensitivity in dynamic indentation. These features also capture trends in Brazilian data, but do not eliminate mesh dependence. Accordingly, advances in modeling and validation are required to develop material models

that are predictive for a variety of loading scenarios using a single parameter set.

Acknowledgements

The authors thank the following individuals for their substantial contributions to the work presented in this paper: David Bronowski, Bill Bruchey, Jerry LaSalvia, Moo Lee, Dave MacKenzie, Herb Miller, Mike Normandia, and John Rowe. Part of this work was performed at the Sandia National Laboratories. Sandia is a multiprogram laboratory operated by Sandia Corporation, a Lockheed Martin Company, for the United States Department of Energy under contract no. DE-ALO4-04AL8500.

References

1. G. R. Johnson and T. J. Holmquist, *A Computational Constitutive Model for Brittle Materials Subjected to Large Strains, High Strain Rates and High Pressures*, Dekker, New York, 1990, 1075 pp.
2. D. Templeton, et al. A Comparison of Ceramic Material Models," *Ceramic Armor Materials by Design*, ed., J. W. McCauley. Vol. 134, 11–18. Ceramic Transactions, Cocoa Beach, FL, 2002.
3. G. E. Hauver, et al. *Interface Defeat of Long-Rod Projectiles by Ceramic Armor*, Army Research Lab, Aberdeen Proving Ground, MD, 2005.
4. P. Lundberg and B. Lundberg, "Transition Between Interface Defeat and Penetration for Tungsten Projectiles and Four Silicon Carbide Materials," *Int. J. Impact Eng.*, 31 [7] 781–792 (2005).
5. D. L. Orphal and R. R. Franzen, "Penetration of Confined Silicon Carbide Targets by Tungsten Long Rods at Impact Velocities from 1.5 to 4.6 km/s," *Int. J. Impact Eng.*, 19 [1] 1–13 (1997).
6. C. E. Anderson, et al., "Re-Examination of the Evidence for a Failure Wave in SiC Penetration Experiments," *Int. J. Impact Eng.*, 33 [1–12] 24–34 (2006).
7. T. J. Holmquist and G. R. Johnson, "Characterization and Evaluation of Silicon Carbide for High-Velocity Impact," *J. Appl. Phys.*, 97 [9] 093502 (2005).
8. E. S. C. Chin and J. W. McCauley, "Armor Materials by Design," *45th Sagamore Conference Proceedings*, ed., J. W. McCauley. Army Research Laboratory, St. Michaels, MD, 1–170, 2001.
9. J. W. McCauley, "Ceramic Armor Materials by Design," *PAC RIM 4*, ed., J. W. McCauley. Vol. 134. Ceramic Transactions, Maui, HI, 113–138, 2002.
10. M. J. Normandia and W. Gooch, *A Overview of Ballistic Testing Methods of Ceramic Materials*, 113–138. PAC RIM 4, Maui, HI, 2001.
11. C. D. Donaldson, R. M. Contiliano, and C. V. Swanson, *The Qualification of Target Materials using the Integral Theory of Impact*, Aeronautical Research Associates of Princeton Inc., Princeton, NJ, 1977.
12. C. D. Donaldson and T. B. McDonough, *A Simple Integral Theory for Impact Cratering by High Speed Particles*, Aeronautical Research Associates of Princeton Inc., Princeton, NJ, 1973.
13. J. Sternberg, "Material Properties Determining the Resistance of Ceramics to High Velocity Penetration," *J. Appl. Phys.*, 65 [9] 3417–3424 (1989).
14. D. A. Shockey, et al., "Particle Impact Damage in Silicon Nitride," *J. Am. Ceram. Soc.*, 73 [6] 1613–1619 (1990).
15. D. K. Kim, C. S. Lee, and Y. G. Kim, *Dynamic Indentation Damage of Ceramics*, 261–268, American Ceramic Society, Maui, HI, 2001.
16. W. Herrmann and A. H. Jones, *Survey of Hypervelocity Impact Information*, MIT Aeroelastic and Structures Research Laboratory, Cambridge, MA, 1961.
17. W. Goldsmith, "Impact, The Theory and Physical Behavior of Colliding Solids," Edward Arnold Publishers, London, 1960.
18. R. L. Martineau, M. B. Prime, and T. Duffey, "Penetration of HSLA-100 Steel with Tungsten Carbide Spheres at Striking Velocities Between 0.8 and 2.5 km/s," *Int. J. Impact Eng.*, 30 [5] 505–520 (2004).

19. B. R. Lawn, "Indentation of Ceramics with Spheres: A Century After Hertz," *J. Am. Ceram. Soc.*, 81 [8] 1977–1994 (1998).
20. W. J. Stronge, *Impact Mechanics*, Vol. 100. Cambridge University Press, New York, 2000.
21. A. C. Fischer-Cripps, *et al.*, "Introduction to Contact Mechanics. Mechanical Engineering Series," *Appl. Mech. Rev.*, 55 [3] B51–B51 (2002).
22. Y. Tanabe, *et al.* *An Overview of Impact Damages in Ceramic Materials—For Impact Velocity Below 2 km/s*, Vol. 19. Tokyo Institute of Technology, Tokyo, Japan, 1994.
23. R. M. Brannon, J. M. Wells, and O. Erik Strack, "Validating Theories for Brittle Damage," *Metall. Mater. Trans. A*, 38 [12] 2861–2868 (2007).
24. R. M. Summers, *et al.*, "Recent Progress in ALEGRA Development and Application to Ballistic Impacts," *Int. J. Impact Eng.*, 20 [6–10] 779–788 (1997).
25. A. F. Fossum and R. M. Brannon, *The Sandia Geomodel: Theory and User's Guide SAND2004-3226*, Sandia National Laboratories, Albuquerque, MN, 2004.
26. R. M. Brannon, "The Influence of Uncertainty in Crack or Slip Plane Orientations On Cracking or Localization Probabilities," *9th ASCE Specialty Conference on Probabilistic Mechanics and Structural Reliability*, eds., S. Wojtkiewicz, J. Red-Horse, and R. Ghanem. American Society of Civil Engineers, Albuquerque, NM, 26–28, 2004.
27. O. E. Strack, R. M. Brannon, and R. P. Jensen, "Spatial Statistics of Material Strength to Address Mesh Dependency of Conventional Damage Models, Part II: Validation and Application," *J. Appl. Phys.*, (2008) in press.
28. W. Weibull, "A Statistical Distribution Function of Wide Applicability," *J. Appl. Mech.*, 18 293–297 (1951).
29. Z. P. Bažant and J. Planas, *Fracture and Size Effect in Concrete and Other Quasibrittle Materials*, CRC Press LLC, Boca Raton, FL, 1998.
30. Z. P. Bažant, "Role of Deterministic and Statistical Length Scales in Size Effect for Quasibrittle Failure at Crack Initiation," *9th International Conference on Structural Safety and Reliability, Safety and Reliability of Engineering Systems and Structures*, eds., G. Augusti and G. I. Schuëller. IOS Press, Rome, Italy, 411–415, 2005.
31. K. Trustum and A. D. S. Jayatilaka, "On Estimating the Weibull Modulus for a Brittle Material," *J. Mater. Sci.*, 14 1080–1084 (1979).
32. F. Zhou and J.-F. Molinari, "Stochastic Fracture of Ceramics Under Dynamic Tensile Loading," *Int. J. Solids Struct.*, 41 6573–6596 (2004).
33. D. E. Grady, "Shock-Wave Properties of Brittle Solids," *Shock Compression of Condensed Matter*, Vol. 370. eds., S. C. Schmidt and W. C. Tao. AIP, Melville, NY, 9–20, 1996.
34. T. J. Vogler, *et al.*, "Hugoniot and Strength Behavior of Silicon Carbide," *J. Appl. Phys.*, 99 [2] 023512 (2006).
35. D. Dandekar, *A Survey of Compression Studies of Silicon Carbide ARL-TR-2695*, Army Research Lab, Aberdeen Testing Ground, NM, 2004.
36. T. J. Holmquist, *et al.* *A Ceramic Armor Material Database A629263*, TA-COM, Warren, MI, 1999.
37. G. R. Johnson and T. J. Holmquist, "An Improved Computational Constitutive Model for Brittle Materials," *AIP Conference Proceeding 1993*, Vol. 309. High-Pressure Science and Technology, 981–984, 1994.
38. J. M. Duncan, "State of the Art: Limit Equilibrium and Finite-Element Analysis of Slopes," *J. Geotech. Eng.*, 122 [7] 577–596 (1996).
39. C. E. Anderson and I. S. Chocron, "Constitutive Model for In-Situ Comminuted Silicon Carbide," *32th International Ceramics and Composites*, ed., L. P. Franks. Ceramic Engineering and Science Proceedings, Daytona Beach, FL, 1280–1286, 2008.
40. R. M. Brannon, M. Y. Lee, and D. R. Bronowski, *Uniaxial and Triaxial Compression Tests of Silicon Carbide Ceramics Under Quasi-Static Loading Condition, SAND2004-6005*, Sandia National Laboratories, Albuquerque, NM, 2005.
41. R. M. Brannon, A. F. Fossum, and O. E. Strack, *Kayenta: Theory and User's Guide*, Sandia National Laboratories, Albuquerque, NM, 2009.
42. R. M. Brannon, O. E. Strack, and M. Y. Lee, "Spatial Statistics of Material Strength to Address Mesh Dependency of Conventional Damage Models, Part I: Theory and Experiment," *J. Appl. Mech.*, (2008) in press.
43. Y. D. Murray, *Users Manual for LS-DYNA Concrete Material Model 159*, FAA report #FHWA-HRT-05-062. Federal Highway Administration, Springfield, VA, 2007.
44. R. M. Brannon, *Aleatory Uncertainty in Simulations of Failure and Fragmentation, Invited Seminar*, Purdue University, West Lafayette, Indiana, 2007.
45. T. J. Vogler, W. D. Reinhart, and L. C. Chhabildas, "Dynamic Behavior of Boron Carbide," *J. Appl. Phys.*, 95 [8] 4173–4183 (2004).
46. M. Timmel, *et al.*, "A Finite Element Model for Impact Simulation with Laminated Glass," *Int. J. Impact Eng.*, 34 1465–1478 (2007).
47. J. C. LaSalvia, *et al.* "Sphere Impact Induced Damage in Ceramics: I. Armor-Grade SiC and TiB₂", *Ceramic Engineering and Science Proceedings*, Vol. 26, Cocoa Beach, FL, 170–181, 2005.
48. J. C. LaSalvia, *et al.* "Sphere Impact Induced Damage in Ceramics: II. Armor-Grade B₄C and WC", *Ceramic Engineering and Science Proceedings*, Vol. 26, Cocoa Beach, FL, 183–192, 2005.
49. H. T. Miller, W. H. Green, and J. C. LaSalvia, "Ballistically Induced Damage in Ceramic Targets as Revealed by X-ray Computed Tomography," *31st International Conference on Advanced Ceramics and Composites*, ed., J. S. Jeffrey. Ceramic Engineering and Science Proceedings, Cocoa Beach, FL, 193–202, 2007.
50. J. M. Duncan, "Friction Angles for Sand, Gravel and Rockfill," *Kenneth L. Lee Memorial Seminar*. Long Beach, CA, 2004.
51. T. J. Holmquist and G. R. Johnson, "Characterization and Evaluation of Boron Carbide for Plate-Impact Conditions," *J. Appl. Phys.*, 100 [9] 093525 (2006).
52. H. Wang and K. T. Ramesh, "Dynamic Strength and Fragmentation of Hot-Pressed Silicon Carbide Under Uniaxial Compression," *Acta Mater.*, 52 [2] 355–367 (2004).
53. B. Paliwal and K. T. Ramesh, "Effect of Crack Growth Dynamics on the Rate-Sensitive Behavior of Hot-Pressed Boron Carbide," *Script. Mater.*, 57 [6] 481–484 (2007).